**Reconstructing regional ionospheric electron density: a combined spherical Slepian function and Empirical Orthogonal Function approach**

Saeed Farzaneh[1], Ehsan Forootan[2]
[1]*Department of Surveying and Geomatics Engineering, University College of Engineering, University of Tehran*
[2]*School of Earth and Ocean Sciences, Cardiff University, UK*
*Email addresses: farzaneh@ut.ac.ir (Saeed Farzaneh), ForootanE@cardiff.ac.uk (Ehsan Forootan)*

**Abstract:**

The Computerized Ionospheric Tomography (CIT) is a method for imaging the Earth's ionosphere using sounding technique and computing the Slant Total Electron Content (STEC) values from data of the Global Positioning System (GPS). The most common approach for ionospheric tomography is the voxel-based model, in which: (i) the ionosphere is divided into voxels, (ii) the STEC is then measured along (many) satellite signal paths, and finally (iii) an inversion procedure is applied to reconstruct the electron density distribution of the ionosphere. In this study, a computationally efficient approach is introduced, which improves the inversion procedure of step (iii). Our proposed method combines the Empirical Orthogonal Function (EOF) and the spherical Slepian base functions to describe the vertical and horizontal distribution of electron density, respectively. Thus, it can be applied on regional and global case studies. Numerical application is demonstrated using the ground-based GPS data over South America. Our results are validated against ionospheric tomography obtained from the COSMIC (Constellation Observing System for Meteorology, Ionosphere, and Climate) observations and the Global Ionosphere Map (GIM) estimated by international centers , as well as by comparison with STEC derived from independent GPS stations. Using the proposed approach, we find that while using 30 GPS measurements in South America, one can achieve comparable accuracy with those from COSMIC data within the reported accuracy ($1\times 10^{11}$ el/cm3) of the product. Comparisons with real observations of 2 GPS stations indicate an absolute difference is less than 2 TECU.

**Keywords:** Computerized Ionospheric Tomography, Slant Total Electron Content (STEC), Slepian base function, Empirical Orthogonal Function (EOF)

## 1. Introduction

The Earth's ionosphere, which is a layer of the ionised gas in the atmosphere (between ~60-2000 km altitude) surrounding the Earth, plays a critical role in satellite communications, as well as space sciences. Generally speaking, when radio waves pass through the ionosphere, both their group phase and velocity are disturbed by free electrons in the ionosphere. The resulting effect in the first approximation is proportional to the Slant Total Electron Content (STEC) along the signal path and is inversely proportional to the frequency (of the group) squared (Hofmann-Wellenhof et al. 2008).

It is well known that the influence of ionosphere on communications systems can be quantified, provided that the distribution of the electron density within the ionosphere is known (Davies 1990). Several methods and instruments are therefore currently being applied to determine the distribution of ionospheric electron density namely techniques that utilize satellites, ionosondes, and incoherent scatter radar data (Zolesi and Cander 2014).

Ionospheric models are divided into three main categories of (i) physical, (ii) empirical, and (iii) mathematical models (see an overview in Figure 1). Physical models try to simulate ionospheric changes based on physical laws or assumptions concerning the processes that cause spatial-temporal variations in the ionosphere, examples include the Global Assimilative Ionospheric Model (GAIM, Schunk et al. 2004). Empirical models, namely the International Reference Ionosphere (IRI, Bilitza et al. 2011) and the NeQuick (Radicella et al. 2009), make use of relationships between solar radiations and the spatial-temporal changes of ions and electrons in ionosphere. Finally, mathematical models that are focused in this paper, are produced by processing of observations derived from, e.g., navigational satellites, and estimating electron distribution within ionosphere by solving an inversion.

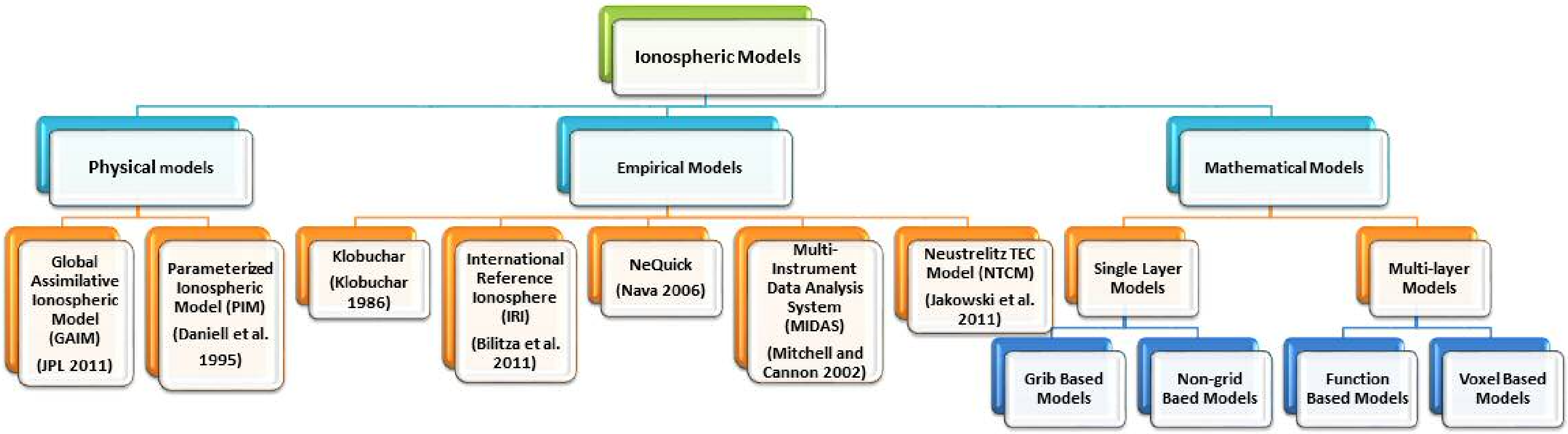


**Figure 1: Classifications of the ionospheric models. For the physical and Empirical models, few examples are introduced. The general structure of mathematical models can be divided into single- and multi-layer structures, whereas each can be formulated using mathematical representation as can be seen in the boxes located at the bottom of this figure.**

State-of-the-art of ionospheric modeling can be treated under either short-time static or dynamic assumption. Both techniques are based on some hypotheses, which bring computational benefits and might also result in limitations. In the short-time static way, one will be able to gather enough observations to perform the inversion but with a central assumption that the state of ionosphere does not change during this time, which is not physically justified. For the dynamic approach (used for near real-time applications), one must rely on a model to introduce dynamics of ionosphere (see e.g. Erdoga et al. 2017). Selecting an appropriate model to introduce the dynamic of ionosphere and its impact on the final results has not been evaluated yet. In this paper, we explicitly focus on the short-time static (or off-line mapping) and try to show how changing base-functions can help improving the inversion and estimation of the ionospheric parameters (Schaer 1999; Schmidt 2007; Schmidt et al.2007; Zeilhofer 2008; Alizadeh et al. 2011).

Concentrating only on the mathematical models, there are several ways to convert observations into the ionospheric parameters. In general, appropriate strategies to implement such conversions depend on the parameterization and dimension of the desired model, as well as its area of coverage. These all together leads to a selection of appropriate base functions that are used to estimate the unknown parameters of the conversion, and finally represent the model. Table 1 summarizes a number of previous studies that apply the 'mathematical method' for ionospheric modeling and the base functions used in them. In the following, details of these selections are described.

STEC provides a valuable source of information about the vertical summation of electrons along the line-of-sight (path between satellite and the in-situ station). Therefore, a tomographic technique is required to detail the distribution of electron density within the ionosphere as a function of space and time. These methods can fall into two categories of iterative and non-iterative techniques. The former was the first choice to solve the ionospheric tomography problem due to its simplicity and low memory requirement following the Algebraic Reconstruction Technique (ART, e.g., Austen et al. 1986). To improve the numerical aspects, ART have found numerous derivatives such as MART (multiplicative algebraic reconstruction technique, Raymund et al. 1993), as well as SIRT (simultaneous iterative reconstruction technique, Afraimovich et al. 1992 and Pryse and Kersley 1992). Yet, dependency on initial values and sensitivity to the level of noise are the main concerns and limitations of the above techniques.

**Table 1: Summary of previous studies that apply mathematical approaches for modeling ionosphere. Base functions that are used to represent corresponding models are also listed.**

<table>
<tr><th>Modeling Dimension</th><th>Parameter</th><th>Coverage</th><th colspan="2">Base Function</th><th>Literature</th></tr>
<tr><td rowspan="3">2D</td><td rowspan="3">$VTEC(\lambda,\varphi)$</td><td>Global</td><td colspan="2">Spherical Harmonics (SH)</td><td>(Schaer 1999)</td></tr>
<tr><td rowspan="2">Regional</td><td colspan="2">2D quadratic B-splines</td><td>(Schmidt et al. 2008)</td></tr>
<tr><td colspan="2">Slepian base Function</td><td>(Sharifi and Farzaneh 2014)</td></tr>
<tr><td rowspan="11">3D</td><td rowspan="4">$VTEC(\lambda,\varphi,t)$</td><td rowspan="2">Global</td><td colspan="2">2D SH + Fourier function for time</td><td>(Alizadeh 2013)</td></tr>
<tr><td colspan="2">trigonometric/ exponential B-splines</td><td>(Alizadeh 2013)</td></tr>
<tr><td rowspan="2">Regional</td><td colspan="2">3D quadratic B-splines</td><td>(Nohutcu et al. 2010)</td></tr>
<tr><td colspan="2">2D Slepian base function+B-spline function for time</td><td>(Sharifi and Farzaneh 2014)</td></tr>
<tr><td rowspan="5">$N(\lambda,\varphi,h)$</td><td colspan="3">Voxels (classical tomography)</td><td>(Garcia-Fernandez et al. 2005)</td></tr>
<tr><td rowspan="2">Global</td><td rowspan="2">2D SH + function for height</td><td>Empirical Orthogonal Function (EOF) for height</td><td>(Liu 2004)</td></tr>
<tr><td>Chapman profile</td><td>(Alizadeh 2013)</td></tr>
<tr><td rowspan="2">Regional</td><td colspan="2">3D B-splines</td><td>(Zeilhofer 2008)</td></tr>
<tr><td colspan="2">2D Spherical Cap Harmonic (SCH)+Empirical Orthogonal Function (EOF)</td><td>(AL-Fanek, 2013)</td></tr>
<tr><td rowspan="3">4D</td><td rowspan="3">$N(\lambda,\varphi,h,t)$</td><td>Global</td><td colspan="2">2D SH + function for height +function for time</td><td>(Alizadeh 2013)</td></tr>
<tr><td rowspan="2">Regional</td><td colspan="2">4D B-splines</td><td>(Schmidt et al. 2011)</td></tr>
<tr><td colspan="2">Chapman Function+Slepian base function</td><td>(Sharifi and Farzaneh 2014)</td></tr>
</table>

By growing the numerical power, non-iterative approaches were formulated for tomographic (3D) modeling of the ionosphere based on stochastic inversion techniques, while using either the voxel-based or function-based approach. In the former category, complex physical interplay between solar radio flux and the Earth's magnetic field is introduced to the inversion using statistical modes of empirical ionospheric models such as the Parameterized Ionospheric Model (PIM) and International Reference Ionosphere (IRI), see for example, Fremouw et al. (1992) and the adopted approach with some modifications in Erturk et al. (2009), Liu and Gao (2004), Mitchell and Spencer (2003), Schmidt (2007), and many others. By employing the function-based approach, the electron distribution in the ionosphere is described by two functions corresponding to the horizontal and vertical changes.

Spherical harmonics (SH) base functions are usually used in previous studies to represent horizontal electron density distribution as long as the modeled area covers the whole sphere and the data is distributed regularly (Chambodut et al. 2005; Mautz et al. 2005; Liu et al. 2006; Schmidt et al. 2007). Vertical changes are accounted for by applying the empirical orthogonal function (EOF) method (see the description of decomposing techniques in Forootan, 2014).

Considering the sampling of STEC observations, application of the SH technique can be limited by the data gaps and inhomogeneous distribution of observations all over the globe. In another words, the SH approach form a well-understood and convenient apparatus to represent and analyze observations globally, but its application is limited to identify the spatial and spectral structure of local anomalies (Beggan et al. 2013; Simons 2010).

In order to mitigate the limitations of SHA, AL-Fanek (2013) applies spherical cap harmonics (SCH) to describe the horizontal distribution of ionospheric electron density, where the vertical component is described based on the EOF technique. Their investigations are performed over the Canadian polar cap, where the spherical cap technique provides a great opportunity by reducing the lack of orthogonality of the global spherical harmonics over local regions. The method, however, requires a symmetric boundary definition when performing the fitting procedure.

In this study, we propose the use of the Slepian base functions to model horizontal ionospheric changes in regions with irregular boundary shapes. This characteristic is important to assess the spectral characteristics of horizontal ionospheric changes in regions with distinct geographical property with less (spectral) contribution from the neighboring regions. In another words, the application of the Slepian base functions reduces the spatial leakage that limits the accuracy of regional ionospheric tomography models.

Application of the Slepian base functions to account for horizontal variability of VTEC was first proposed by Sharifi and Farzaneh (2014). This selection is motivated by the fact that less number of unknown parameters required to model the horizontal changes of ionosphere, compared to the spherical harmonics and the spherical cap base functions. As a result, the computational load is reduced and the localized signal is more efficiently retrieved thanks to the regional representation of the Slepian base functions. In another attempt, Etemadfard and Hossainali (2015) applied these base functions to improve the accuracy of the IGS global ionosphere models (GIMs) in the polar regions. Particularly, they compare measures of the spatial resolution derived from the modified model (solved by Slepian base function) and original GIMs, as well as their biases. Their results indicate that the Slepian base functions are regionally optimized and well suited to model the ionosphere. Once the suitability of these base functions established, the method is applied by e.g., Etemadfard and Hossainali (2016) for VTEC modeling in the Arctic region. We should mention here that the proposed Slepian base functions of this study are not only efficient to solve regional ionospheric tomography problems, but also, they are also likely beneficial in global case studies. In fact, in a global case, one can show that Slepian base functions are linearly related to a combination of spherical harmonics. However, in contrast to the spherical harmonics, the Slepian base functions can be concentrated over regions with large signal magnitudes, while preserving their orthogonality over the entire sphere, and maximize their recovery within as inversion (Wieczorek and Simons, 2005; Simons et al., 2006). An appropriate selection of the location of Slepian base functions, for example along the boundary of the study region, also improves the localization of inverted solutions, and consequently, reduces the spatial leakage errors. This benefit is illustrated in various case studies, for example, in a seismic modelling application (Wang, 2012) or a similar application on applying radial base function for global gravity field modelling as in Yang et al. (2017). Application of the Slepian base functions for a global ionospheric tomography application will be addressed in future.

It is worth reminding that in the most of previous studies, researches focus on an off-line signal processing to generate STEC tomography with the main assumption that the state of ionosphere does not change dramatically over a certain time-period, for example, 2 hours in the IGS products (Schaer et al., 1998). This assumption often provides a reliable opportunity to gather enough GNSS observations to perform inversion, thus, this view has also been followed in this study Simlar to Sharif and Farzaneh (2014), the EOF technique is applied to describe the vertical distribution of ionospheric electron density. Recently, Erdogan et al. (2017) suggest a near real-time formulation to model global VTEC, where they use B-Splines to model horizontal changes in ionosphere and a Kalman filtering approach to account for ionosphere's temporal variations. An extension of the suggested inversion formulation to be used for near real-time applications will be addressed in future.

In this study, we use GPS-derived STEC measurements are used that cover the southern part of America during 17 March 2013 (with maximum solar activity) and 21 December 2013 (with moderate solar activity). The developed function-based tomographic modeling system has been compared with results from the Constellation Observing System for the Meteorology, Ionosphere and Climate (COSMIC) observations and the Global Ionosphere Maps (GIM), as well as by comparison with STEC derived from independent GPS stations.

## 2. Method

### 2.1. STEC determination

In this work, STEC are estimated from the differential code delay and carrier phase measurements on both the L1 and L2. For this purpose, the carrier-to-code leveling process method (Ciraolo et al. 2007; Nohutcu et al. 2010) is utilized. The necessary equations can be extracted from Sharifi and Farzaneh (2014).

### 2.2. Spherical Slepian base functions

Slepian base functions (Slepian 1983) are band-limited harmonics with the maximum degree $L$, and at the same time are spatially concentrated inside a target region. Therefore, they can be defined as a particular linear combination of the spherical harmonics. However, unlike the spherical harmonics that are globally defined, they can be arranged according to their energy concentration inside the target region (Simons et al. 2006). Therefore, a signal of interest $g$ in the location $r$ can be mathematically defined as

$$g(r) = \sum_{l=0}^{L} \sum_{l=-m}^{m} g_{lm} Y_{lm}(r), \tag{1}$$

where $Y_{lm}(\mathrm{r})$ is a real spherical harmonic of degree $l$ and order $m$, while $r$ is the location of a point on the surface of the unit sphere $\Omega$ and $g_{lm}$ has been defined as:

$$g_{lm} = \int_{\Omega} g(r) Y_{lm}(r)\, \mathrm{d}\,\Omega. \tag{2}$$

To maximize the spatial concentration of the band-limited function $g(r)$ within the region $R$, the ratio of the norms should be maximized as:

$$\lambda = \max \frac{\int_R g^2(\Omega) d\Omega}{\int_{\Omega_G} g^2(\Omega) d\Omega}, \tag{3}$$

where $0 \leq \lambda \leq 1$ is a measure of the spatial concentration. The maximization of this concentration criterion can be achieved in the spectral domain by solving the algebraic eigenvalue problem [Simons et al. 2006]:

$$Dg = \lambda g, \tag{4}$$

where the elements of $(L+1)^2 \times (L+1)^2$ localizing kernel $D$ :

$$
D=\begin{bmatrix}
D_{0,0;0,0} & \cdots & D_{0,0;L,0} & D_{0,0;1,-1} & \cdots & D_{0,0;L,-1} & D_{0,0;1,1} & \cdots & D_{0,0;L,1} & \cdots & D_{0,0;L,L}\\
\vdots & & & & & & & & & & \vdots\\
D_{L,0;0,0} & \cdots & D_{L,0;L,0} & D_{L,0;1,-1} & \cdots & D_{L,0;L,-1} & D_{L,0;1,1} & \cdots & D_{L,0;L,1} & \cdots & D_{L,0;L,L}\\
D_{1,-1;0,0} & \cdots & D_{1,-1;L,0} & D_{1,-1;1,-1} & \cdots & D_{1,-1;L,-1} & D_{1,-1;1,1} & \cdots & D_{1,-1;L,1} & \cdots & D_{1,-1;L,L}\\
\vdots & & & & & & & & & & \vdots\\
D_{L,-1;0,0} & \cdots & D_{L,-1;L,0} & D_{L,-1;1,-1} & \cdots & D_{L,-1;L,-1} & D_{L,-1;1,1} & \cdots & D_{L,-1;L,1} & \cdots & D_{L,-1;L,L}\\
D_{1,1;0,0} & \cdots & D_{1,1;L,0} & D_{1,1;1,-1} & \cdots & D_{1,1;L,-1} & D_{1,1;1,1} & \cdots & D_{1,1;L,1} & \cdots & D_{1,1;L,L}\\
\vdots & & & & & & & & & & \vdots\\
D_{L,1;0,0} & \cdots & D_{L,1;L,0} & D_{L,1;1,-1} & \cdots & D_{L,1;L,-1} & D_{L,1;1,1} & \cdots & D_{L,1;L,1} & \cdots & D_{L,1;L,L}\\
\vdots & & & & & & & & & & \vdots\\
D_{L,L;0,0} & \cdots & D_{L,L;L,0} & D_{L,L;1,-1} & \cdots & D_{L,L;L,-1} & D_{L,L;1,1} & \cdots & D_{L,L;L,1} & \cdots & D_{L,L;L,L}
\end{bmatrix}, \tag{5}
$$

Which are obtained by:

$$
D_{lm,l'm'}=\int_R Y_{lm}(\Omega)Y_{l'm'}(\Omega)\,\mathrm{d}\,\Omega, \tag{6}
$$

and $g$ is the $(L+1)^2$ dimensional vector that represents the Slepian eigenfunction expressed by spherical harmonics, i.e.

$$
g=(g_{00}\ldots g_{lm}\ldots g_{LL})^T. \tag{7}
$$

This ‘localization’ matrix is symmetric and the subspace of maximum energy is obtained by solving an eigenvalue decomposition (Simons 2010). When the signal $g(r)$ is local, it can be approximated using the Slepian expansion truncated at the Shannon number $N$ (Percival and Walden 1993):

$$
N=\sum_{n=1}^{(L+1)^2}\lambda_n=(L+1)^2\frac{A}{4\pi}, \tag{8}
$$

where $A$ is the area of region as a solid angle relative to the full sphere. The data can be approximated with very good reconstruction properties within the region by:

$$
d(\hat{r})\approx\sum_{n=1}^{N}d_n g_n(\hat{r}), \tag{9}
$$

where $g_n(\hat{r})$ and $d_n$ are the spherical Slepian base function and unknown coefficients, respectively (Simon 2010).

### 2.3. Modeling the Ionosphere

The ionospheric delay in the GPS signals observed by the ground stations can be converted into STEC, which is the total number of electrons in a column of unit cross-section between the satellite and the receiver on the ground. The mathematical representation of the definition is:

$$STEC = \int_{R}^{S} N_e(r,\theta,\varphi,t)ds, \tag{10}$$

where $N_e$ is the electron density at time $t$, $ds$ is the geometric range along the signal path between the satellite and the receiver, $\theta, \lambda$ are longitude and latitude, and $STEC$ is the slant total electron content, respectively (Liu and Gao 2003). A common way of discretizing Eq. (10) is to divide the ionosphere into a grid of three-dimensional volume pixels, also known as voxels, which are set up in a way that each voxel is bounded in pre-defined latitude, longitude and altitude with the electron density assumed to be homogeneous within each voxel. By this assumption, Eq. (10) can be expressed as follows (AL-Fanek 2013):

$$STEC = \sum_{i=1}^{N_\lambda} \sum_{j=1}^{N_\varphi} \sum_{k=1}^{N_h} N_{e_{i,j,k}} \Delta h_{i,j,k} \delta_{i,j,k}, \tag{11}$$

with

$$\delta_{i,j,k} = \begin{cases} 1 & ray\ in\ voxel \\ 0 & other\ wise \end{cases}, \tag{12}$$

where $\Delta h_{i,j,k}$ is the ray path length in the voxel i, j, k and $N_\lambda$, $N_\varphi$ and $N_h$ are the number of voxels in the longitude, latitude and height direction, respectively. In Eq. (11), $N_{e_{i,j,k}}$ represents the electron density in the voxel i, j, k. Therefore, Eq. (11) can be expressed as:

$$STEC = A.N_e, \tag{13}$$

where $A$ is the design matrix, $N_e$ is the vector of the electron density to be estimated. Entries of the design matrix are the path length of the satellite-to-receiver signal propagating through each voxel.

Since observations are usually not well distributed, matrix $A$ in Eq. (13) is singular and therefore $N_e$ cannot be estimated from Eq. (13). Besides, the inversion in Eq. (13) is high dimensional, because in a traditional voxel-based formulation of the tomography problem, density coefficients of the 3-D voxels that cover the area and sorted between the Earth's surface and satellite orbits, must be estimate. To mitigate this problem, we re-write Eq. (13) based on orthonormal basis functions, where the unknowns are only the coefficients of the three-dimensional orthonormal basis functions. Therefore, here, the multi-layer three-dimensional modeling of the electron density is derived as:

$$N_e(\lambda,\varphi,h) = \sum_{k=1}^{K}\sum_{n=1}^{N} d_{n,k}\, g_n(\lambda,\varphi) Z_k(\lambda,\varphi,h), \tag{14}$$

where $g_n(\lambda,\varphi)$ is the spherical Slepian base function, $d_n$ represent unknown coefficients, $Z_k(\lambda,\varphi,h)$ stands for empirical orthogonal functions, $K$ is the number of EOFs in the modeling process, and $N$ is the Shannon number representing the maximum degree of the Slepian base functions. The EOFs in Eq. (14) are known and estimated from the International Reference Ionosphere (IRI) model (AL-Fanek 2013). As a result, Eq. (14) can be expressed in the matrix form as:

$$N_e = B.x, \tag{15}$$

where $B$ contains the base functions generated using the EOFs and Slepian base functions expansion, and $x$ is a $(N \times K) \times 1$ vector that contains the tomography model coefficients to be estimated. It is noteworthy that, in this study, we only use the GPS observations, which change through the time. Our central assumption is that within 2 hours time, ionosphere is static and coefficients that correspond to the mentioned base functions will be estimated. In other words, in our formulation, the base functions remains time-invariant, but the observation vector is updated every 2 hours.

A proper value for the Shannon number (N) in Eq. (14) depends on the distribution of input data. For example, Schmidt et al. (2011, 2015) provide a detailed comparisons between spherical harmonics, B-Spline, and wavelet techniques. In this study, first Slepian eigenfunctions and their eigenvalues for the region of interest are estimated. Consequently, the dominant eigenfunctions that correspond to the normalized singular values of $\lambda \geq 0.5$ are considered well distinguished from the rest. The number of dominant base-functions can be related to N in Eq. (14) using the approach presented in Simons (2010), from which N = 21 is found to be most of the time an optimum value and a trade-off between the resolution level and the computational load (see similar arguments in Erdogan et al., 2017). The number of EOFs (K) in Eq. (14) can be chosen by applying statistical tests as demonstrated by Forootan (2014, chapter 3). Here we followed the dominant variance portion approach to choose K, where often K=3 is found to represent 99% of variance in the vertical direction.

Substituting Eq. (15) in Eq. (13), the ionospheric tomography problem can be expressed as follows:

$$STEC = G.x, \tag{16}$$

where

$$G = \mathrm{A}.B. \tag{17}$$

The unknown tomography model coefficients in Eq. (16) can be obtained using the least-squares method. The design matrix $G$ in Eq. (16) is ill-conditioned. In order to achieve reasonable estimates, the generalized Tikhonov regularization (Tikhonov 1963) has been applied for which, the L-curve method has been used to determine the optimum regularization parameter. Nevertheless, an application of a regularization likely yields biased solutions that are smoother than those derived from an 'ordinary' least squares (if the latter was possible to be computed). In this study, we follow the methodology in Shen et al. (2012), to minimize the regularization bias. Figure 2 shows a schematic diagram of the proposed method for estimating ionospheric tomography using Slepian base functions.

In Section 3, we further compare the resulting maps with independent data, which justifies the accuracy of the implemented inversion in Eq. (16).

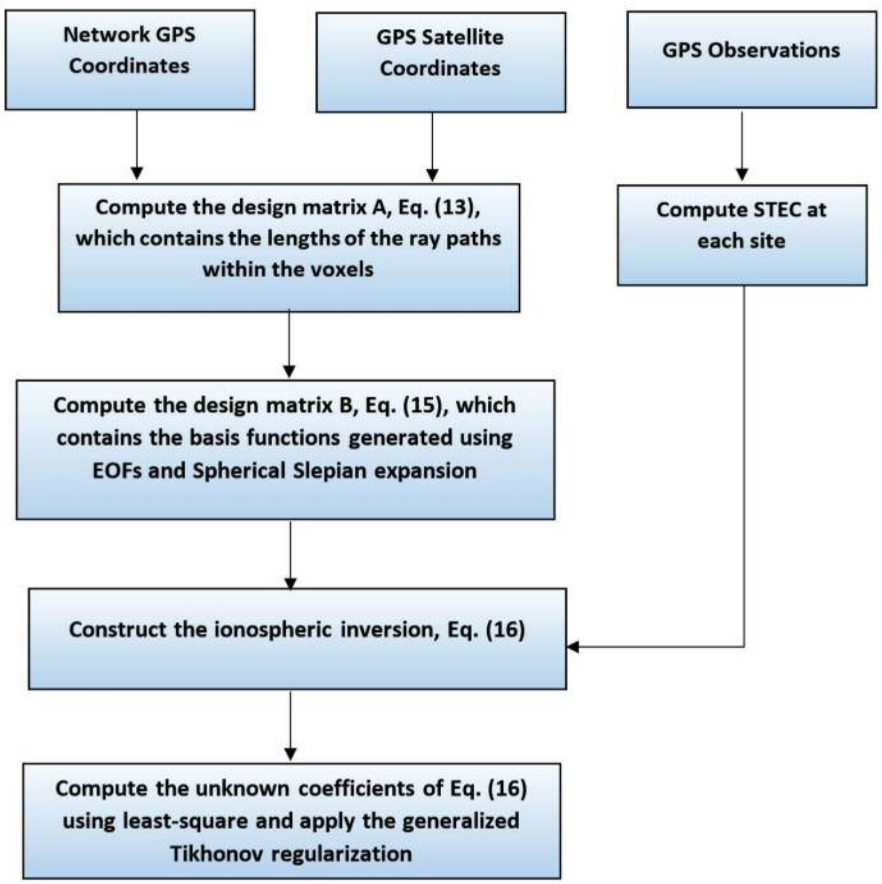


**Figure 2: Flowchart of the ionospheric tomography inversion using in-situ GNSS data and Slepian base functions**

## 3. Results and discussion

The computerized ionospheric tomography in this study is based on the ground-based GPS observations collected across South American. The 24h observations of 30 stations belong to International GNSS Service (IGS) and Brazilian Network for continuous GPS Monitoring (RBMC) networks are obtained from www.ibge.gov.br with the sampling rate of every 30 s. The geographical region used in this work extends from $20^\circ$ S to $40^\circ$ S in latitude, $280^\circ$ E to $320^\circ$ E in longitude and 80 km to 1200 km in altitude and the spatial resolution along the longitude, latitude and altitude is considered $1^\circ \times 2^\circ \times 10km$ . The resolution is chosen according to the number and quality of observations and it is also selected in a way to be better than those of the International GNSS Service (IGS) maps (Schaer et al., 1998). Thus, the total numbers of voxels in the region is 49392. Classically, to estimate STEC, one needs to compute one parameter per voxel, which makes the least squares system extremely unstable. However, by reformulating the inversion using Slepian base functions and EOFs, reflected in Eq. (14), the number of unknowns is reduced to 63. The number of observations is based on time period and the number of GPS satellites. Here similar to the IGS strategy (Schaer et al., 1998), the inversion is estimated to generate 2-hourly maps. Spatial distribution of the stations and ionospheric observables are illustrated in Figure 3.

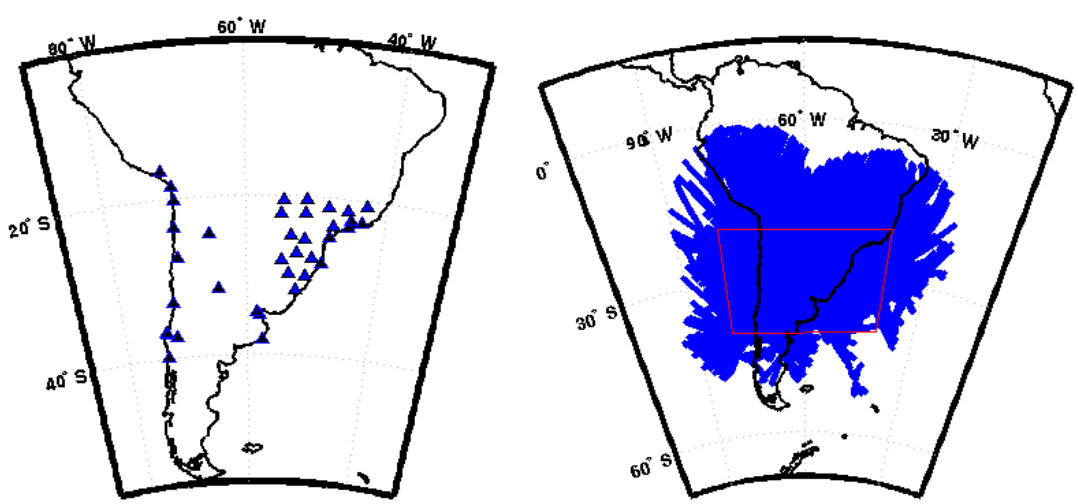


**Figure 3: Left: distribution of the 30 GPS reference stations, Right: distribution of ionospheric observable (blue dots) and voxel boundaries (red)**

In order to solve STEC from observations, the receiver Inter-Frequency Biases (IFBs) are calculated using the Bernese GPS software v 5.0, and the IFB values for the satellite are obtained from the Center of the Orbit Determination in Europe (CODE). The STEC values for each observation are computed as described in Sharifi and Farzane (2014). The precise orbit files, provided by several IGS agencies, are interpolated, using the Lagrange method, to determine the satellite positions. These STEC measurements contain the ionospheric electron density information above the GPS network, therefore they are used as the input data for our ionospheric electron density modeling.

To develop the tomographic model of South America, the ionosphere is assumed to be constant within two hour and the EOF analysis is perform within that hour. Figure 4 illustrates the first three EOFs, which represent 99 percent of variance of electron density in the vertical from 00:00 UT to 01:00 UT, December 21, 2013. Similar results are derived for March 17, 2013. They are not however shown here.

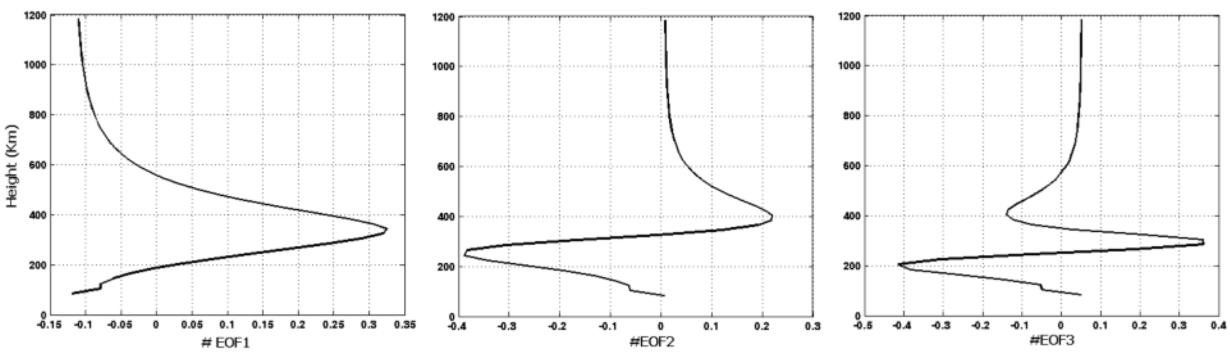


**Figure 4: First three EOFs derived from IRI-2012 model**

The EOFs along with Slepian base functions are used to depict the ionosphere field in a 3D model using Eq. (16). It is well known that the parameters of the Earth's ionosphere are strongly controlled by solar and magnetic activity, which can be indicated by e.g., the Kp-index (Liu et al. 2006). Therefore, to demonstrate the performance of the proposed technique, our model is validated under different quiet and active ionospheric conditions. Figure 5 shows the geomagnetic conditions for 17 March 2013 (with maximum solar activity) and 21 December 2013 (with moderate solar activity).

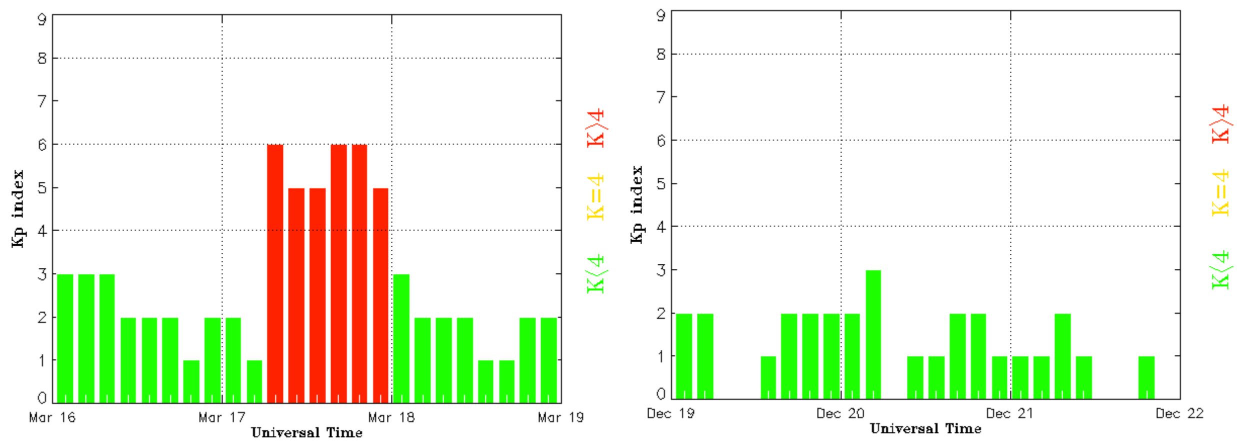


**Figure 5: The estimated planetary K index for (left): Year 2013 Day Number 355, (right): Year 2013 Day Number76 (http://www.spaceweatherlive.com).**

The assessment of the accuracy was made in several ways. First, the CIT-estimated vertical TEC maps for 17 March and 21 December 2013 are presented in Figures 6 and 7 for the mid-point of the modeling period. The vertical TEC maps are obtained by integrating through the CIT-estimated electron density profiles as follows:

$$TEC(\lambda_i,\varphi_i) = 10^{-16} \times \Delta height \times \sum_{j=1}^{number\ of\ vertical\ layers} N_e(\lambda_i,\varphi_i,h_j), \tag{18}$$

where the units of the electron density ( $N_e$ ), and the voxel size in height ( $\Delta height$ ) are $el/m^3$ and $m$ respectively. As expected, the results follow the variation trend in the IRI-2012 model. The ionosphere maximum, which appears around local noon as travelling along with the Sun, is clearly visible in the VTEC maps. The results on 17 March 2013 indicate a minimum VTEC of ~19 around 8h AM and ~ 30 around 5h PM (see Figure 6). An average value of VTEC during March of a year with normal magnetic activity is ~15-20. The bigger values estimated here clearly indicate the impact of higher magnetic activity during this day. On 21 December 2013, a minimum VTEC of ~15 around 8h AM and ~50 around 16h PM are found (see Figure 7), which is in a normal range during this time of year. We repeat this experiment using the traditional voxel-based inversion technique using $2^\circ \times 2^\circ \times 45km$ voxels (, which its corresponding inversion system in more stable than the high resolution $1^\circ \times 1^\circ \times 10km$ voxels). Our results (not shown here) indicate that the proposed formulation of this paper increases the chance of producing TEC closer to the actual VTEC value from GPS observations by 37%.

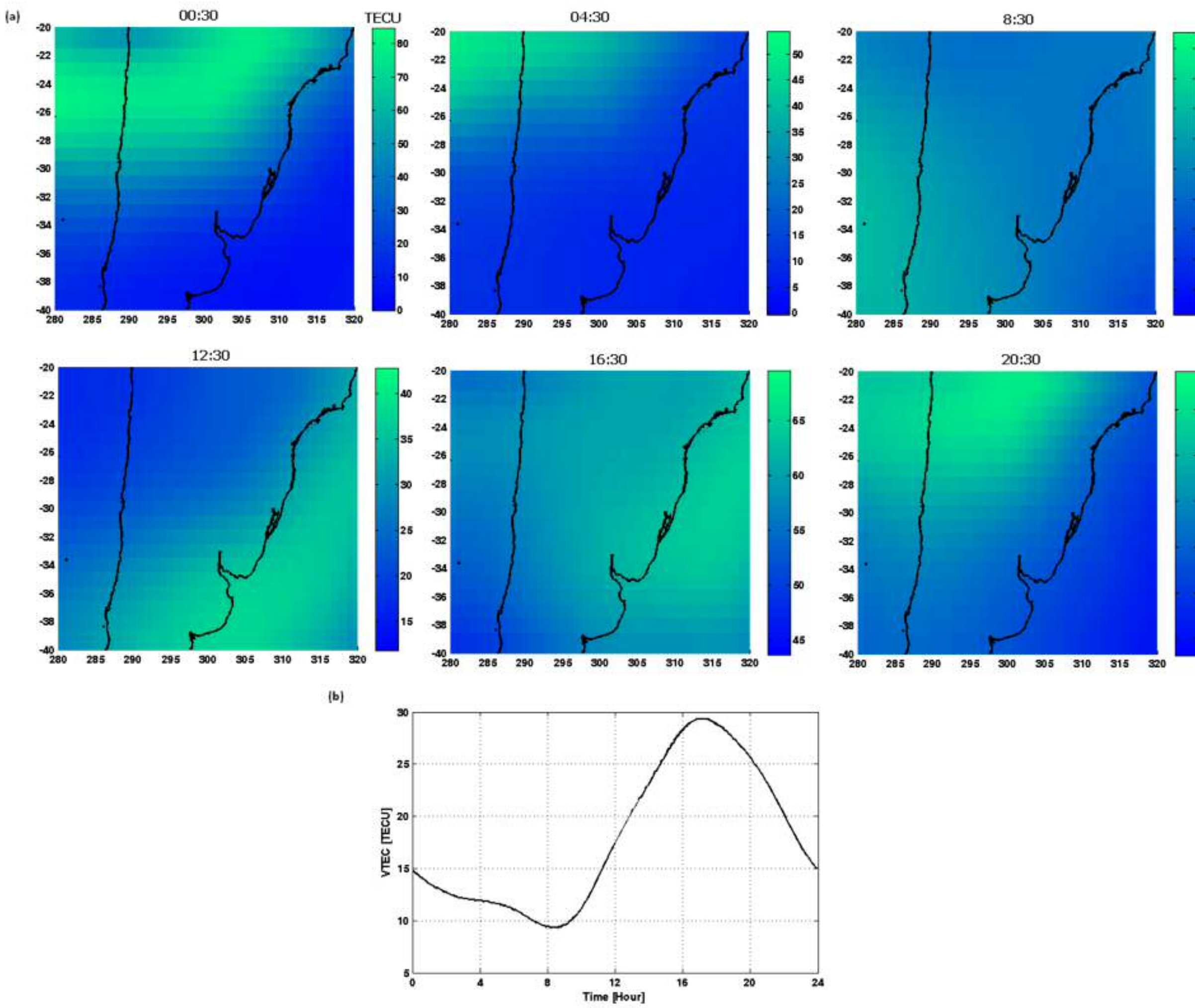


**Figure 6: a:) Estimated vertical TEC maps for 17 March 2013, b:) reference diurnal IRI-TEC variation**

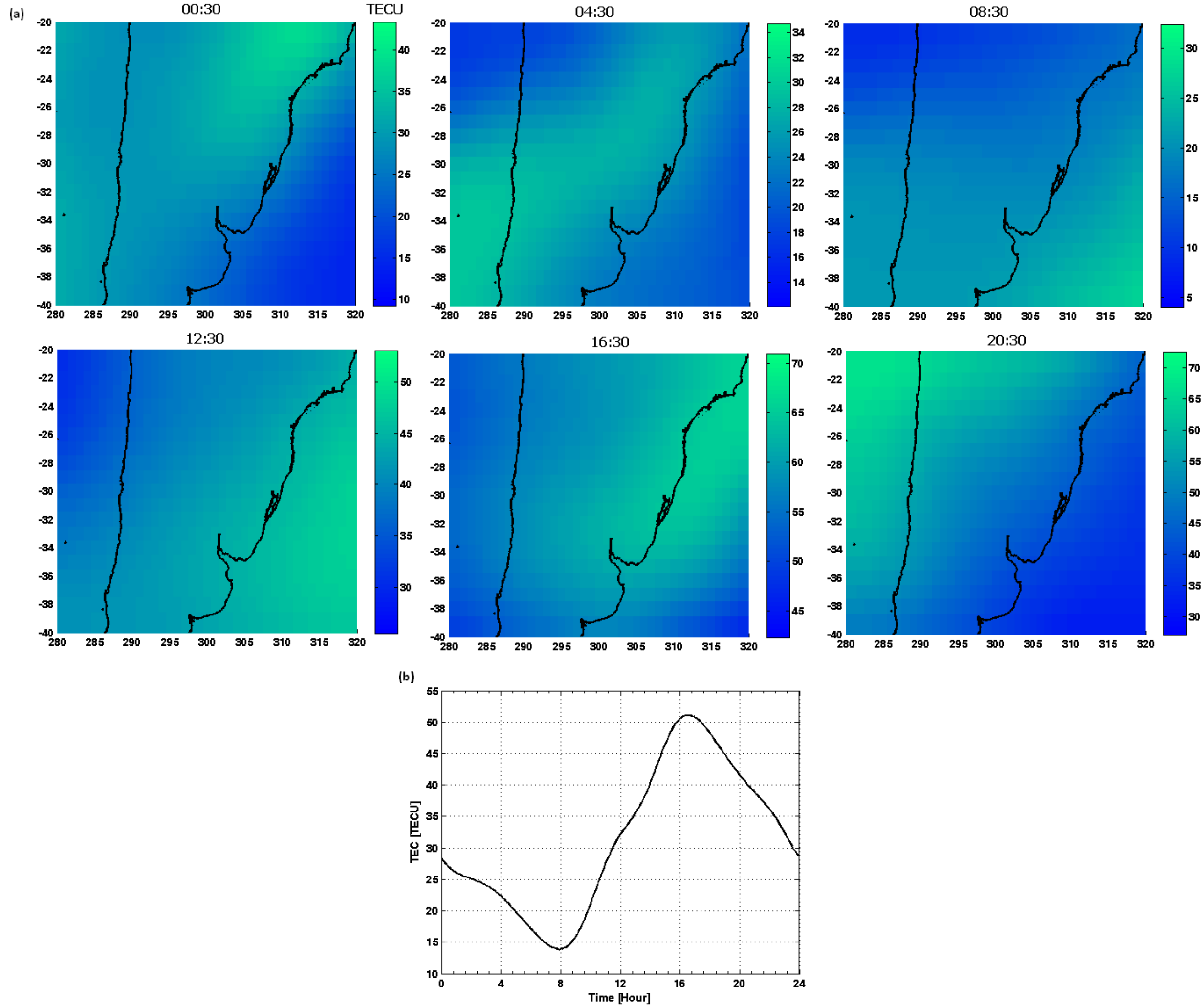


**Figure 7: a:) Estimated vertical TEC maps for 21 December 2013, b:) reference diurnal IRI-TEC variation**

As our second assessment, the CIT derived electron density profile is compared to the one derived using the radio occultation measurements. The FORMOSAT-3/COSMIC (F/C) constellation of 6 satellites was launched on 15 April, 2006. Their initial orbit was at an altitude of 500 km, but they were gradually raised to an altitude of 800 km. There is $30^\circ$ separation between the satellites with an orbital period of 100 min (Feng 2010; Liou et al. 2007). More than 3 million ionospheric profiles have been provided by the COSMIC working group (http://cosmic-io.cosmic.ucar.edu/). In this study, the second level data "ionprf files" are used that contain information about ionospheric electron densities. The data are provided by CDACC (http://www.cosmic.ucar.edu) with a reported accuracy of $1\times10^{11}$ el/cm$^3$

(COSMIC Program Office Website, 2013). This accuracy has been used as a reference of the accuracy measure of the radio occultation retrieved electron density profiles.

Before evaluating the proposed method with RO data, it is necessary to perform some quality control tests on the individual ionospheric electron density profiles. For this purpose, a two-layer Chapman function described in Lei et al. (2007) is fitted to each profile using the least-squares method. This yields the best match with RO electron density profiles at F2 region. Furthermore, in order to quantitatively assess the effect of ionospheric plasma irregularities on the height variation of the electron density, we estimate mean deviation of the electron density profiles following Yang et al. (2009).

Figure 8 illustrates the two COSMIC samples related to an unsuitable (left) and a suitable (right) electron density profile. The accepted electron density profiles (passed the quality control tests) are used to validate our reconstructed results derived from the proposed ionospheric tomographic technique.

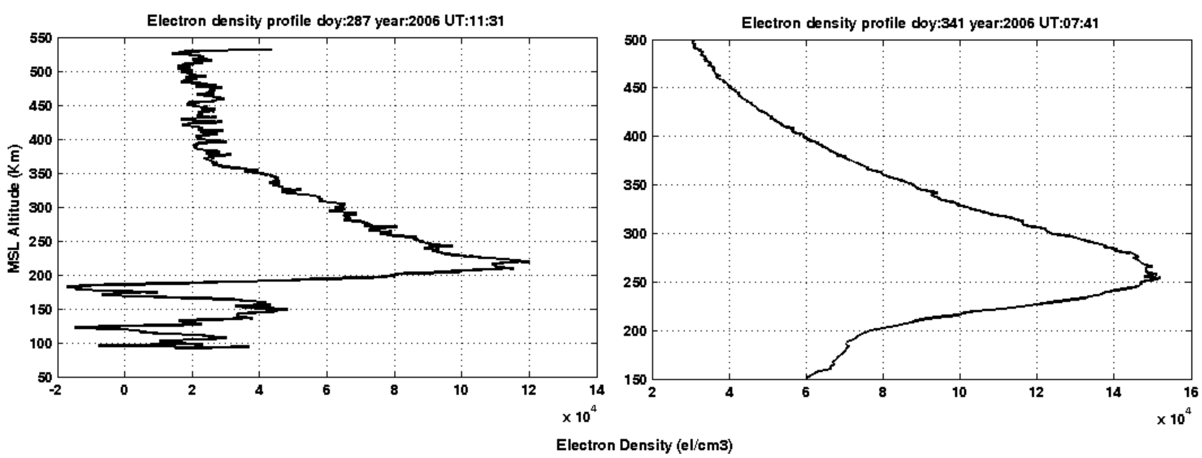


**Figure 8: Left: the failed electron density profile; Right: the accepted electron density profile observed by FORMOSAT-3/COSMIC and used in our quality control tests.**

Figure 9 shows footprints of all F/C occultation measurements through the whole days 17 March and 21 December 2013.

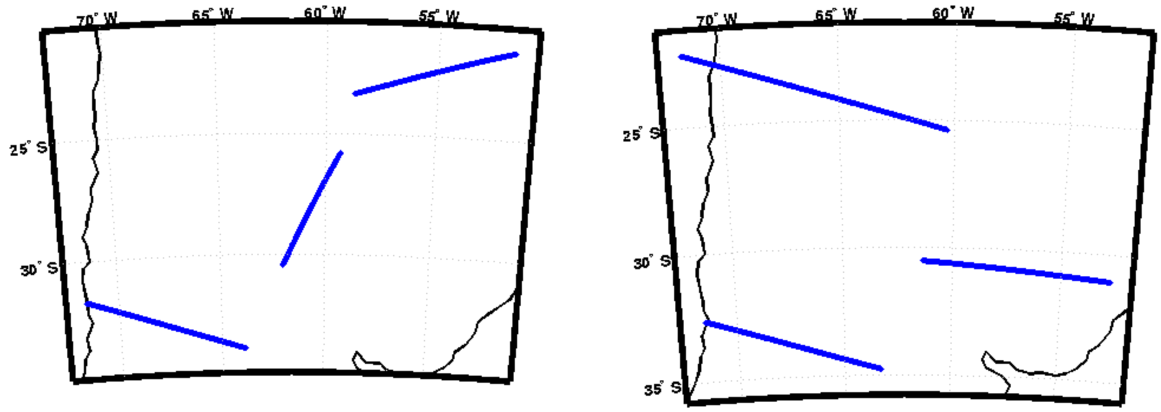


**Figure 9: Left: Footprints of F/C occultation measurements for 21 December 2013, Right: Footprints of F/C occultation measurements for 17 March 2013.**

Figures 10 and 11 show the difference between the two derived profiles. The red line represents the accuracy range ( $\pm 1 \times 10^{11}$ el/cm3) of the radio occultation derived electron density profile, as mentioned before. The CIT-derived electron density is defined at the center of each voxel. To better compare and validate the results, the CIT-derived profiles are interpolated and the electron density profiles are computed at the geographical coordinates of the radio occultation perigee points. Errors of a full day of radio occultation events are estimated and summarized in Table (2). The root mean square (rms) error determines how much the calculated data deviates from the observed data, in other words, how well the derived or calculated data fit the measured data. The results indicate that overall pattern of our model predictions is very close to measurements (RMSE of $\sim 0.6 \times 10^{11} el / m^3$ ) although imperfect fitting points can be found, e.g., at around of F2 layer. This behavior could be explained by the fact that during maximum solar activity the ionosphere is very variable to such an extent that the variation of the electron density with time might be nonlinear over the period of inversion. As a result, any short-time static inversion methodology, including the one proposed here, fails to reflect the temporal non-linearity of ionosphere. This might be improved by a dynamic formulation of the proposed inversion, which will be discussed in future.

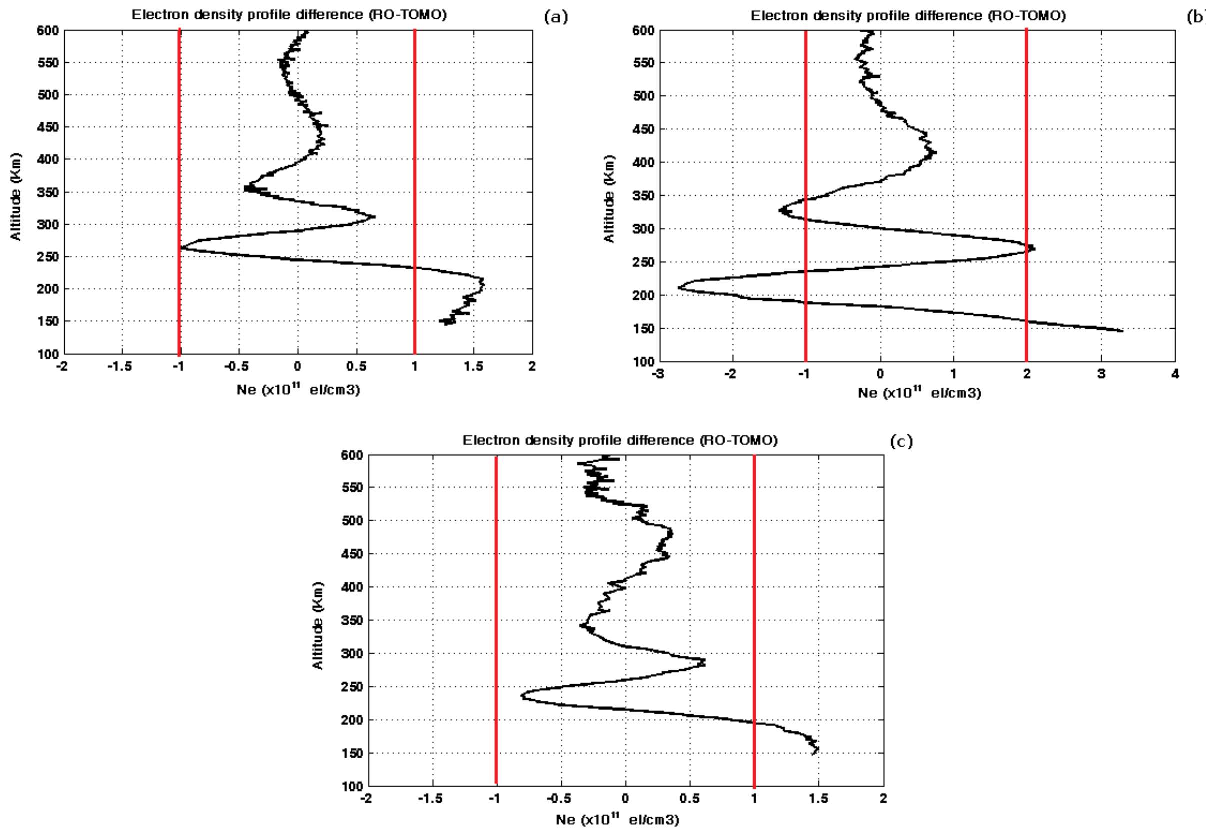


**Figure 10: Electron density profiles differences between Radio occultation (RO) and tomography electron density profiles for 21 December 2013 a:) 16.57 (UTC) b:) 08.49 (UTC) c:) 10.32 (UTC)**

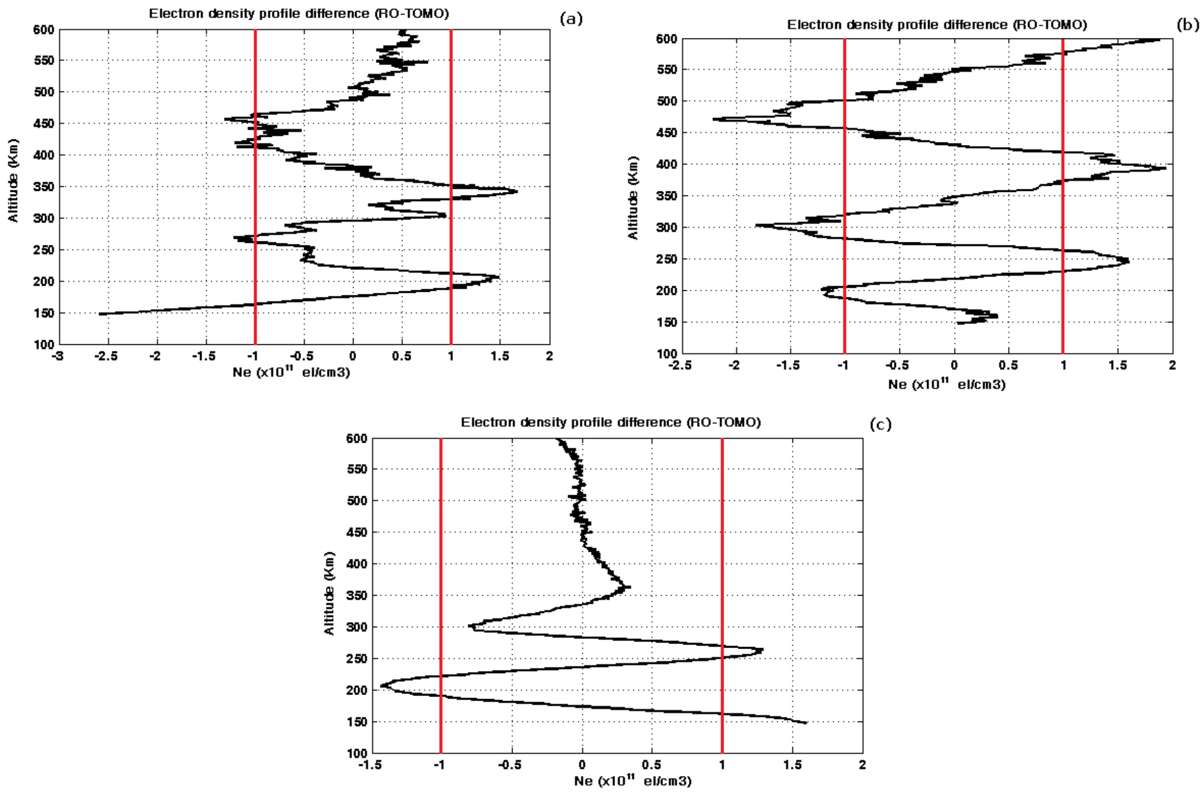


**Figure 11: Electron density profiles differences between Radio occultation (RO) and tomography electron density profiles for 17 March 2013 a:) 16.52 (UTC) b:) 16.55 (UTC) c:) 13.26 (UTC)**

Table 2: Summary of the statistics of the difference between the electron density profiles derived by radio occultation vs. CIT

| **Date** | **RMSE ($10^{11}$ el/m$^3$)** |
|---|---|
| **21 December 2013** | 0.43 |
| **17 March 2013** | 0.58 |

As a third evaluation, we compare the results of our proposed method with the VTEC estimates derived from the CODE, ESA and IGS centers (Schaer 1999). Figure 12 shows the results for the test point arbitrary located at latitude $\varphi = -30^{\circ}$ and longitude $\lambda = 300^{\circ}$ for 17 March and 21 December 2013 and Table (3) describes the estimated error statistics. The overall patterns of the VTEC are found to be similar. Range of VTEC from these global models are found to be different than the values generated by our regional inversion (computed using Eq. (18)). This difference could be related to the global nature of these models and the fact that they try to represent VTEC globally rather than being sensitive to local fluctuations. Should these results be taken into account, it can be concluded that the proposed algorithm has the high capability in the local modeling of VTEC, with profiles following expected diurnal TEC variations with low nighttime TEC values and midday peaks and displaying no negative TEC values.

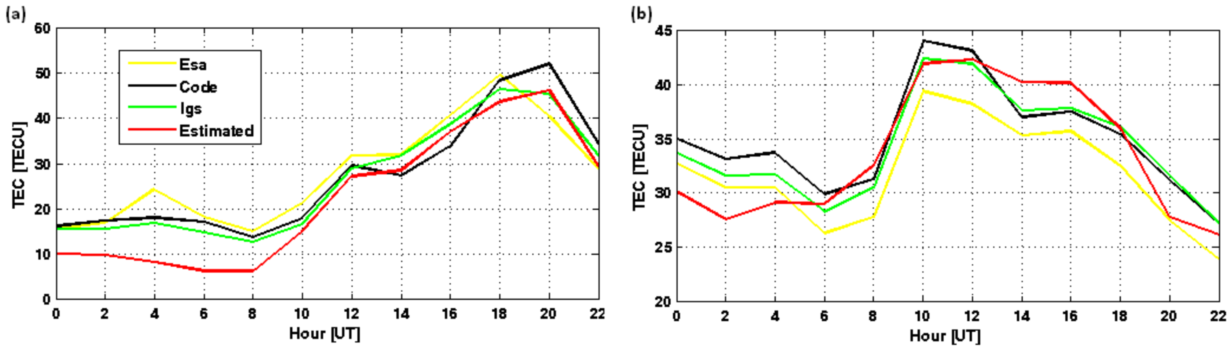


**Figure 12: The comparison of the predicted TEC with the estimated value by CODE, ESA and IGS for a) 17 March 2013 and b) 21 December 2013.**

Table 3: Summary of the statistics of the difference between the estimated TEC with the estimated value by CODE, ESA and IGS

| | **21 December 2013** | |
|---|---|---|
| **Date** | **STD (TECU)** | **Mean (TECU)** |
| **predicted TEC- the estimated value by CODE** | 2.8803 | -6.7842 |
| **predicted TEC- the estimated value by ESA** | 2.8138 | -3.6092 |
| **predicted TEC- the estimated value by IGS** | 2.3839 | -6.1175 |
| | **17 March 2013** | |
| **predicted TEC- the estimated value by CODE** | 4.1374 | -4.8592 |
| **predicted TEC- the estimated value by ESA** | 5.5458 | -5.5758 |
| **predicted TEC- the estimated value by IGS** | 2.9425 | -3.9592 |

To further validate the proposed model, it is necessary to verify the reliability of the CIT model using real observations. In this experiment, observations of 2 GPS stations belong to the Brazilian Network for Continuous Monitoring of the GNSS Systems (RBMC http://www.ibge.gov.br/english/geociencias/geodesia/rbmc/rbmc.shtm) are used for validation. These stations are not involved in the inversion of this study thus can be used as an external assessment to calculate the STEC on signal propagation paths. The mean and RMS of the errors for two selected stations during the two selected days in March and December are listed in Tables (4). The reconstruction results are found to be close to those from these 2 stations, where the absolute difference is found to be less than 2 TEC unite (TECU). Bigger errors are found during high geomagnetic activity in March, compare the results in Table 4. We estimate the bias of solutions following Shen et al. (2012). Our numerical results indicate that this impact is very marginal, i.e., maximum values are found to be 0.073 TECU, while comparing the solutions with VTEC from GPS measurements.

Table 4: Summary of the statistics of differences between the estimated TEC and observations at two stations, whose observations are not used during the inversion

| **21 December 2013** | | |
|---|---|---|
| **Station** | **STD (TECU)** | **Mean (TECU)** |
| *Ourinhos (latitude -22.95, Longitude310.1)* | 0.9424 | 0.9632 |
| *Santa Maria (latitude -29.7167, Longitude306.2833)* | 0.6341 | 0.6902 |
| **17 March 2013** | | |
| *Ourinhos (latitude -22.95, Longitude310.1)* | 0.8763 | 1.7897 |
| *Santa Maria (latitude -29.7167, Longitude306.2833)* | 0.6667 | 1.4373 |

#### 4. Summary and conclusion

The aim of this paper was to determine the suitability of the ionospheric tomography as a tool to determine the electron density profiles using GPS data. To achieve this, a new three-dimensional Computerized Ionospheric Tomographic technique is developed, in which a combination of spherical Slepian base functions and empirical orthogonal functions (EOFs) is used to describe the electron density distribution. The spherical Slepian base functions describe the electron distribution horizontally and the empirical orthogonal functions represent the electron density distribution vertically. Various comparisons with independent data and model simulations such as Radio Occultation observations, VTEC profiles from the International GNSS Service (IGS) models, and external GPS stations are performed to demonstrate the feasibility and performance of the technique under different ionospheric conditions. Particularly, we test the estimated ionospheric profiles during two different days with high ( $K_p > 4$ ) and low ( $K_p < 4$ ) solar activity. Our results indicate that the electron density profiles are fairly well comparable with the RO derived profiles from the Constellation Observing System for Meteorology, Ionosphere, and Climate (COSMIC) observations within the reported accuracy of the product ( $1 \times 10^{11}$ el/cm$^3$). Comparisons with the IGS's Global Ionosphere Maps (GIM) confirm that the developed tomographic model predicts ionosphere without unexpected oscillations, though the range of variations from IGS models is found to be underestimated. Comparing the reconstructed results with real observations of 2 GPS stations within the region indicates an absolute difference is less than 2 TECU, which indicates a high correspondence.

Ionospheric imaging using tomography is an ill-posed inverse problem. Various reasons might contribute in the quality of the solution of this inversion, which includes the number, quality, and distribution of observations, as well as parameterization and computation strategy used for this inversion. For example, lack of GPS observations in the in oceans and seas or the poor geometry of observed signals over certain regions makes modelling the ionosphere using GNSS data alone very difficult. Besides, since gathering observations over all possible angles is rare, there are insufficient measurements perpendicular to altitude and therefore the vertical resolution is not as good as horizontal. These issues impose certain limitations in the resolution and accuracy of ionospheric tomography solutions. To mitigate these limitations, one might use some a priori information such as data/model derived empirical orthogonal functions to improve the vertical distribution of electron density. In addition, incorporating other data sources might help improving horizontal and vertical resolution. For example, satellite-based observations such as those from F/C provide additional observations with good vertical coverage, which can be used to help number of observations of the topside ionosphere data. The Galileo, GLONASS and Beidou are examples of other constellations that can improve the quantity of TEC data, increasing the data coverage for the proposed inversion. Further investigations should be conducted for different wide area GPS networks at different latitudes with higher reference station density with longer period data coverage. Investigations should be added to address feasibility of the proposed technique and the effect of different parameters on the model accuracy. Although the main product of the model is electron density, TEC maps can be computed and ionospheric corrections for navigation applications can be generated. The quality of these maps and hence the ionospheric correction is expected to be better than the conventional TEC maps generated from two-dimensional modelling.

**Acknowledgements**. The authors are grateful to Professor M. Rycroft and two reviewers for their comments, which helped us to improve this manuscript. We would like to acknowledge (1) the NASA's Archive of Space Geodesy Data (CDDIS, http://cddis.gsfc.nasa.gov) and Instituto Brasileiro de Geografia e Estatística (IBGE, http://www.ibge.gov.br) for the RINEX data (2) the NPSO (Taiwan's National Space Organization) and UCAR

(University Center for Atmospheric Research) for access the COSMIC RO data (http://cdaac-www.cosmic.ucar.edu/cdaac/products.html).

**References**

Alizadeh, M.M., H. Schuh, S. Todorova, and M. Schmidt (2011), Global Ionosphere Maps of VTEC from GNSS, Satellite Altimetry and Formosat-3/COSMIC Data, Journal of Geodesy 85(12), 975-987.

Afraimovich EL, Pirog OM, Terekhov AI (1992), Diagnostics of large-scale structures of the high-latitude ionosphere based on tomographic treatment of navigation-satellite signals and of data from ionospheric stations. Journal of Atmospheric and Terrestrial Physics, Vol. 54 No. 10, pp. 1265–1273.

Alizadeh MM (2013) Multi-Dimensional modeling of the ionospheric parameters, using space geodetic techniques. PhD thesis, Vienna University of Technology, Geowissenchaftliche Mitteilungen Heft Nr. 93, 2013, ISSN 1811-8380.

Al-Fanek, OJS (2013), Ionospheric Imaging for Canadian Polar Regions, Ph.D. dissertation, Department of Geomatics Engineering UCGE Reports NO. 20383, University of Calgary.

Austen JR, Franke SJ, Liu CH, Yeh KC (1986), “Application of computerized tomography techniques to ionospheric research”, Presented at the International Beacon Satellite Symposium on Radio Beacon Contribution to the Study of Ionization and Dynamics of the Ionosphere and to Corrections to Geodesy and Technical Workshop, pp. 25–35.

Beggan C, Saarimaki J Whaler K, Simons F (2013), Spectral and spatial decomposition of lithospheric magnetic field models using spherical Slepian base functions. Geophysical Journal International 193: 136-148.

Bilitza D, McKinnell L, Reinisch B Fuller-Rowell T (2011). The international reference ionosphere today and in the future. J. Geod., 85, 909 - 920.

Chambodut A, Panet I, Mandea M, Diament M Holschneider M, Jamet O (2005), Wavelet frames: an alternative to spherical harmonic representation of potential fields. Geophysical Journal International 163, 875–899.

Ciraolo L, Azpilicueta F, Brunini C, Meza A, Radicella SM (2007), Calibration errors on experimental Slant Total Electron Content (TEC) determined with GPS. Journal of Geodesy 81 (2), 111–120.

"COSMIC Program Office Website". (2013), Retrieved from http://cdaac-www.cosmic.ucar.edu/cdaac/products.html.

Davies K (1990). Ionospheric radio (No. 31). IET.

Daniell R, Brown L, Anderson D, Fox M, Doherty P, Decker D, Sojka J, Schunk R (1995). Parameterized ionospheric model: A global ionospheric parameterization based on rst principles models. Radio Sci., 30, 1499-1510.

Erturk O, Arikan O Arikan F (2009), Tomographic reconstruction of the ionospheric electron density as a function of space and time. Advances in Space Research, Vol. 43 No. 11, pp. 1702–1710.

Etemadfard H, Hossainali MM (2015) Application of Slepian theory for improving the accuracy of SH-based global ionosphere models in the Arctic region. J Geophys Res Space Phys. doi:10. 1002/2015JA021811

Etemadfard H, Hossainali MM (2016) Spherical Slepian as a new method for ionospheric modeling in arctic region. J Atmos Solar Terr Phys 140:10–15. doi:10.1016/j.jastp.2016.01.003.

Erdogan, E., Schmidt, M., Seitz, F., Durmaz, M. (2017). Ann. Geophys., 35, 263 -277, doi:10.5194/angeo-35-263-2017, https://www.ann-geophys.net/35/263/2017/angeo-35-263-2017.pdf

Feng M (2010) Detection of high-latitude ionospheric irregularities from GPS radio occultation. MSc diss., University of Calgary.

Fremouw EJ, Secan JA, Howe BM (1992), "Application of stochastic inverse theory to ionospheric tomography", Radio Science, Vol. 27 No. 5, pp. 721–732.

Forootan, E. (2014) Statistical signal decomposition techniques for analyzing time-variable satellite gravimetry data. PhD thesis, University of Bonn. http://hss.ulb.uni-bonn.de/2014/3766/3766.pdf.

Garcia-Fernandez M, Hernandez-Pajares M, Juan J, Sanz J (2005). Performance of the improved abel transform to estimate electron density pro_les from GPS occultation data. GPS Solut, 9, 105 - 110.

Hofmann-Wellenhof B, Lichtenegger H Wasle E (2008), GNSS – Global Navigation Satellite Systems – GPS, GLONASS, Galileo & more., Springer-Verlag, Wien.

Jakowski N, Hoque M, Mayer C (2011). A new global TEC model for estimating transionospheric radio wave propagation errors. J. Geod., 85, 965-974.

Klobuchar J (1986). Design and characteristics of the GPS ionospheric time-delay algorithm for single-frequency users. In PLANS'86 - Position Location and Navigation Symposium, 280-286, Las Vegas, Nevada.

Lei J, Syndergaard S, Burns AG, Solomon SC, Wang W, Zeng Z et al (2007). Comparison of COSMIC ionospheric measurements with ground-based observations and model predictions: Preliminary results. Journal of Geophysical Research, 112, A07308.

Liou YA, Pavelyev AG, Liu SF, Pavelyev AA, Yen N, Huang CY et al (2007). FORMOSAT-3/COSMIC GPS radio occultation mission: preliminary results. IEEE Transactions on Geoscience and Remote Sensing, 45(11), 3813-3826.

Liu Z (2004) Ionospheric tomography modeling and application using global positioning system (GPS) measurements. Ph.D dissertation, Department of Geomatics Engineering, University of Calgary.

Liu Z, Gao Y (2003), Ionospheric TEC predictions over a local area GPS reference network. GPS Solutions 8 (1), 23-29.

Liu Z Gao Y (2004), “Development and Evaluation of a New 3-D Ionospheric Modeling Method”, Navigation, Vol. 51 No. 4, pp. 311–329.

Liu Z, Skone S, Gao Y (2006),Assessment of ionosphere tomographic modeling performance using GPS data during the October 2003 geomagnetic storm event, Rsdio Science, 41, RS1007, doi:10.1029/2004RS003236.

Liu L, Wan W, Ning B, Pirog OM, Kurkin VI (2006), Solar activity variations of the ionospheric peak electron density, J. Geophys. Res., 111, *A08304, doi:*10.1029/2006JA011598.

Mautz R, Ping J, Heki K, Schaffrin B, Shum CK, Potts L (2005) Efficient spatial and temporal representations of global ionosphere maps over Japan using B-spline wavelets. Journal of Geodesy 78, 660–667.

Mitchell C, Cannon P (2002). Multi-instrumental data analysis system (MIDAS) imaging of the ionosphere. Tech. rep., University of Bath, United States Air Force European Office of Aerospace Research and Development.

Mitchell CN, Spencer PSJ (2003), A three-dimensional time-dependent algorithm for ionospheric imaging using GPS. Annals of Geophysics, 46 (4):687-696.

Nava B (2006). A near real-time model-assisted ionosphere electron density retrieval method. Radio Science.

Nohutcu M, Karslioglu MO, Schmidt MB (2010), B-spline modeling of VTEC over Turkey using GPS observations. Journal of Atmospheric and Solar-Terrestrial Physics 72, 617–624.

Percival DB, Walden AT (1993), Spectral Analysis for Physical Applications, Multitaper and Conventional Univariate Techniques. Cambridge Univ. Press: New York.

Pryse SE, Kersley L (1992), A preliminary experimental test of ionospheric tomography. Journal of Atmospheric and Terrestrial Physics, Vol. 54 No. 7–8, pp. 1007–1012.

Radicella S (2009). The NeQuick model genesis, uses and evolution. ANNALS OF GEOPHYSICS, 52, 417 - 422.

JPL (2011). JPL - NASA, GAIM introduction.Website, http://iono.jpl.nasa.gov/gaim/intro.html.

Raymund TD, Pryse SE, Kersley L, Heaton JaT (1993), Tomographic reconstruction of ionospheric electron density with European incoherent scatter radar verification. Radio Science, Vol. 28 No. 5, pp. 811–817.

Schaer S (1999). Mapping and predicting the Earth's ionosphere using the Global Positioning System. Ph.D. thesis, Bern University, Switzerland.

Schaer, S., Gunter, W. and Feltens, J. (1998). Ionex: The ionosphere map exchange format version 1. In In J. M. Dow, J. Kouba, and T. Springer (Eds.), 233 { 247, Proceeding of the IGS AC Workshop, Darmstadt, Germany.

Schmidt, M., D. Bilitza, C.K. Shum, and C. Zeilhofer, (2007), Regional 4-D modeling of the ionospheric electron content. Advances in Space Research 42, 782–790.

Schmidt, M., Dettmering, D., Mößmer, M., Wang, Y., and Zhang ,J. (2011) Comparison of spherical harmonic and B spline models for the vertical total electron content, Radio Sci., 46, RS0D11, doi:10.1029/2010RS004609.

Schmidt, M., Dettmering, D., and Seitz, F. (2015) Using B-Spline Expansions for Ionosphere Modeling, in: Handbook of Geomathematics ,edited by: Freeden, W., Nashed, M. Z., and Sonar, T., 939-983, doi:10.1007/978-3-642-54551-1_80, Springer Berlin Heidelberg, Berlin, Heidelberg.

Schmidt M (2007), "Wavelet modelling in support of IRI", Advances in Space Research, Vol. 39 No. 5, pp. 932–940.

Schmidt M, Dettmering D, Mossmer M, Wang Y, Zhang J (2011). Comparison of spherical harmonics and B-spline models for the vertical total electron content. Radio Science, 46, RS0D11.

Schmidt M, Fengler M, Mayer-Gurr T, Eicker A, Kusche J, Sanchez L, Han SC (2007), Regional gravity modeling in terms of spherical base functions. Journal of Geodesy 81, 17–38.

Schmidt M, Karslioglu M, Zeilhofer C eds. (2008). Regional multidimensional modeling of the ionosphere from satellite data. TUJK Annual Scienti_c Meeting, Ankara.

Sharifi MA, Farzaneh S (2014). The spatio-spectral localization approach to modeling VTEC over the western part of the USA using GPS observations. Advances in Space Research, 54(6), 908-916.

Shen Y, Xu P, Li B (2012). Bias-corrected regularized solution to inverse ill-posed models. Journal of Geodesy, 86(8), 597-608.

Simons FJ, Dahlen FA, Wieczorek MA (2006), Spatiospectral Concentration on a Sphere. Society for Industrial and Applied Mathematics Review 48: 504-536.

Simons FJ (2010), Slepian base Functions and Their Use in Signal Estimation and Spectral Analysis. In Handbook of Geomathematics, edited by W. Freeden, M.Z. Nashed, and T. Sonar, 891–923, Springer: Berlin.

Slepian D (1983), Some comments on Fourier-analysis, uncertainty and modeling, SIAM Rev., 25(3), 379–393.

Schunk R (1988). A mathematical model of the middle and high latitude ionosphere. Pure Appl. Geophys, 128, 255.

Tikhonov AN (1963). Solution for incorrectly formulated problems and the regularization method. Soviet Math Dokl 4:1035–1038.

Wang L (2012). Coseismic Deformation Detection and Quantification for Great Earthquakes Using Spaceborne Gravimetry. The Ohio State University.

Wieczorek, M.A., Simons F.J (2005), Localized spectral analysis on thesphere, Geophys. J. Int., 162(3), 655–675.

Yang KF, Chu YH, Su CL, Ko HT, Wang CK (2009), An examination of FORMOSAT-3/COSMIC ionospheric electron density profile: data quality criteria and comparisons with the IRI model. Terrestrial, Atmospheric and Oceanic Sciences 20: 193–206.

Yang F, Kusche J, Forootan E, Rietbroek R (2017), Passive-ocean radial basis function approach to improve temporal gravity recovery from GRACE observations, J. Geophys. Res. Solid Earth, 122, 6875–6892, doi:10.1002/2016JB013633.

Zeilhofer C (2008) Multi-dimensional B-spline modeling of spatio-temporal ionospheric signals. Deutsche Geodätische Kommission bei der Bayerischen Akademie der Wissenschaften.

Zolesi B, Cander LR (2014), Ionospheric prediction and forecasting. Heidelberg: Springer.